Advances in Water Resources 16 (1993) 277–284

A control-volume finite-element model for two-dimensional overland flow

G. Gottardi

Istituto di Scienze Minerarie, Università di Bologna, Bologna 40136, Italy

&

M. Venutelli

Istituto di Costruzioni Idrauliche, Università di Bologna, Bologna 40136, Italy

A control-volume finite-element (CVFE) formulation for the numerical integration of the two-dimensional diffusion hydrodynamic model is presented. Three different methods for computing the transmissivity terms are compared on the basis of the global boundary-outflow error for both the finite-element (FE) and the CVFE formulation of the model. As is well known, the two-dimensional diffusion-hydrodynamic model (DHM) is obtained from the more general overland-flow model, based on momentum and mass-balance equations, with inertia terms neglected. The applied CVFE technique uses linear triangular finite-element shape functions to estimate the value of the variables at the boundaries of the subcontrol volume of each node. The use of linear-interpolation functions allows the elemental matrices of the model to be expressed in a simple polynomial form. Integration in time is obtained by a finite-difference (FD) Picard scheme. Some numerical examples are presented to compare, on the basis of global-outflow errors and analytical solution, the performances of six schemes of the CVFE method with that of the equivalent Galerkin FE formulations.

Key words: overland unsteady flow, two-dimensional diffusion model, control-volume finite-element model.

1 INTRODUCTION

The possibility of modeling flooding over catchment basins and water-flow rate into draining-channel networks allows better intervention strategies to be singled out for improving the containing and discharging systems of the superficial water downflow. Two-dimensional unsteady-state models have been applied for studying problems of propagation in shallow water. The numerical integration of the Saint Venant equations governing surface flow in shallow waters has been widely treated in the scientific literature for both one- and two-dimensional cases (Abbott,[1] Chow & Ben-Zvi,[3] Cunge *et al.*,[5] Fennemma & Chaudry[7], Henderson,[11] Katopodes & Strelkoff[14,15]).

In this work, we assume, as proposed by Xanthopoulos and Koutitas[18], that the flood-plain flow regime is such that the inertia terms are negligible in the Saint Venant equations. This simplifying hypothesis leads to the so-called diffusion-hydrodynamic-flow model that is mathematically represented by a parabolic quasi-linear partial differential equation. Hromadka *et al.*[12] presented a two-dimensional FD and a nodal-domain-integration (NDI) FE method for the integration of the DHM. Moreover, the integrated finite difference version of the NDI method was used by De Vries *et al.*[6] and by Hromadka *et al.*[13]

In the NDI method, herein called the CVFE method, the variables in each triangular finite element are supposed to vary linearly in space. By using the classical linear shape functions for the interpolation of the variables, and associating a subcontrol volume to each node of the triangular element, the DHM equation can be expressed in an intuitive physical form for each node of the triangle. The CVFE method, equivalent in its lumping alternative to the integrated finite differences (IFD) of Narasimhan and Witherspoon,[16] was recently applied by Forsyth,[8] Fung *et al.*,[9] and Gottardi and Dall'Olio.[10]

Advances in Water Resources 0309-1708/94/$07.00

In this paper, we compare, on the basis of global boundary outflow, six formulations of the CVFE method, and six corresponding versions of the FE Galerkin method, for the numerical integration of the two-dimensional DHM. The twelve formulations were obtained by using three methods for the interpolation of the transmissivity term hk, and using lumping or not-lumping alternatives.

2 MATHEMATICAL FORMULATION OF THE TWO-DIMENSIONAL DIFFUSION MODEL

The Saint Venant equations for two-dimensional unsteady flow consists of an equation of continuity:

$$\frac{\partial}{\partial x_1}(u_1 h) - \frac{\partial}{\partial x_2}(u_2 h) - \frac{\partial H}{\partial t} = q_e \tag{1}$$

and two motion equations:

$$\frac{\partial}{\partial t}(u_1 h) + \frac{\partial}{\partial x_1}(u_1^2 h) + \frac{\partial}{\partial x_2}(u_1 u_2 h) - gh\frac{\partial h}{\partial x_1} = gh(S_{o_1} - S_{f_1}) \tag{2a}$$

$$\frac{\partial}{\partial t}(u_2 h) + \frac{\partial}{\partial x_2}(u_2^2 h) + \frac{\partial}{\partial x_1}(u_1 u_2 h) + gh\frac{\partial h}{\partial x_2} = gh(S_{o_2} - S_{f_2}) \tag{2b}$$

where u_1 and u_2 indicate average flow velocities along the water depth h in the x_1 and x_2 directions. The parameter H ($H = z - h$) represents the water-surface elevation, z the bed elevation, and q_e the source term (positive if entering the system); S_{o_1}, S_{o_2}, S_{f_1}, and S_{f_2} are, respectively, the bed and the friction slopes in the x_1, x_2 directions, and g and t are the gravitational acceleration and time, respectively.

By substituting in eqns (2a) and (2b), m_i for the sum of the first three terms divided by gh, these equations may be written as:

$$m_i - \frac{\partial H}{\partial x_i} - S_{f_i} = 0 \qquad i = 1,2 \tag{3}$$

We assume that the friction slopes may be approximated by Manning's formula

$$S_{f_i} = \frac{u_i u_s n_i^2}{h^{4/3}} \qquad i = 1,2 \tag{4}$$

where n_1 and n_2 are the Manning roughness coefficients in the x_1 and x_2 directions and u_s is the flow velocity along the direction of the maximum slope. Now, by neglecting the inertia terms m_i, as proposed by Xanthopoulos and Koutitas[18] and Akan and Yen,[2] eqn (3) can be rewritten as:

$$u_i = -k_i \frac{\partial H}{\partial x_i} \qquad i = 1,2 \tag{5}$$

where:

$$k_i = \frac{h^{\frac{5}{3}}}{n_i} \frac{1}{\partial H / \partial s^{\frac{1}{2}}} \qquad i = 1,2 \tag{6}$$

s being the direction of the maximum slope, which makes an angle $\alpha = \tan^{-1}(u_2/u_1)$ in the positive x_1 direction. In the case of an isotropic medium, $k_1 = k_2$.

The two-dimensional DHM is obtained by substituting the motion equation eqn (5), into the continuity equation, eqn (1):

$$\sum_{i=1}^{2} \frac{\partial}{\partial x_i}\left(hk_i \frac{\partial H}{\partial x_i}\right) + q_e = \frac{\partial H}{\partial t} \tag{7}$$

The introduction of the appropriate initial and boundary conditions uniquely defines the mathematical model.

3 NUMERICAL FORMULATION OF THE MODEL

By discretizing the flow domain Ω by a set of n_e triangular subdomains Ω^e so that $\Omega = \cup_{e=1}^{n_e} \Omega^e$, the mass-balance equation, eqn (7), for each subcontrol volume Ω_l^e ($l = n, p, q$) associated with Ω^e (see Fig. 1), may be written as:

$$\int_{\Gamma_l^e} \sum_{i=1}^{2} hk_i \frac{\partial H}{\partial x_i} \nu_i \, ds - \int_{S_l^e} \sum_{i=1}^{2} hk_i \frac{\partial H}{\partial x_i} \nu_i ds - \int_{\Omega_l^e} q_e d\omega = \int_{\Omega_l^e} \frac{\partial H}{\partial t} d\omega \tag{8}$$

where Γ_l^e and S_l^e indicate, respectively, the internal and external boundaries of the subcontrol volume Ω_l^e (e.g. for $l = n$, $\Gamma_n^e = e_p + e_q$ and $S_n^e = nm_q - nm_p$). The parameters ν_1, ν_2 are the direction cosines with respect to x_1 and x_2 of the outward normal to the contour of Ω_l^e, and e_n, e_p, and e_q are the segments connecting the baricenter γ with the mid-points of each side (points m_n, m_p, and m_q) of the triangle Ω^e.

The first two integrals on the left-hand side of eqn (8) take into account, respectively, the mass of water entering Ω_l^e from the internal boundary Γ_l^e and the external boundary S_l^e, whereas the third integral takes into account the external source/sink term. The flow along the boundary S_l^e gives no contribution to the mass of water entering the whole control volume associated

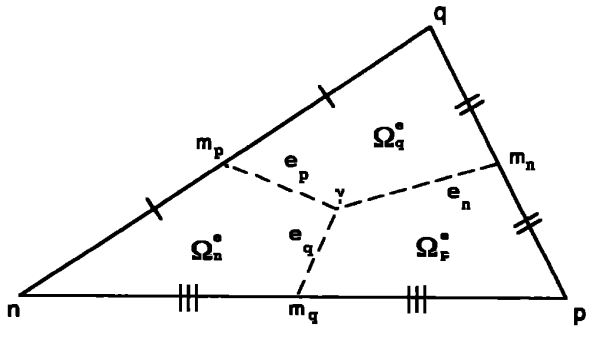

Fig. 1. Basic triangular-mesh element.

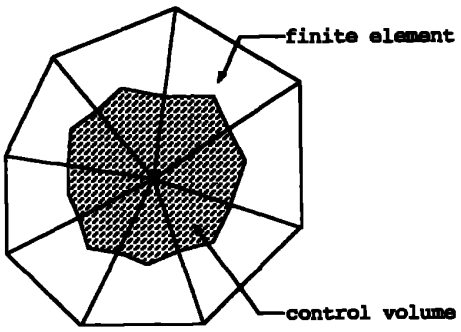

Fig. 2. Control volume associated with a node in a triangular finite-element mesh.

with each node of Ω^e (see Fig. 2), so that, for the subelements that are internal to Ω, it can be neglected. The term on the right hand-side of eqn (8) represents the accumulation of water inside Ω_i^e.

If we indicate by $f(\mathbf{x}, t)$ one of the variables h, k_i, and H inside Ω^e, these quantities can be expressed either as a linear combination of the products of nodal-interpolation functions N_i^e (Connor & Brebbia[4]) by nodal value f_i:

$$f(\mathbf{x}, t) \simeq \hat{f}(\mathbf{x}, t) = \sum_{i=n,p,q} f_i(t) N_i^e(\mathbf{x}) \tag{9a}$$

or as its nodal average value

$$f(\mathbf{x}, t) \simeq \bar{f}(\mathbf{x}, t) = \tfrac{1}{3} \sum_{i=n,p,q} f_i \tag{9b}$$

By using for the variables h, k_i, and H the approximations expressed by eqn (9a), eqn (8) may be written in the following form:

$$-\int_{\Gamma_i^e} \sum_{i=1}^{2} hk_i \frac{\partial N_m^e}{\partial x_i} \nu_i ds \cdot H_m - \int_{\Omega_i^e} N_m^e d\omega \cdot \dot{H}_m = -\int_{S_i^e} q_b ds + \int_{\Omega_i^e} q_e d\omega \qquad l, m = n, p, q \tag{10a}$$

where

$$q_b(x_1, x_2, t) = -\sum_{i=1}^{2} hk_i \frac{\partial H}{\partial x_i} \nu_i$$

The Galerkin weak-form of eqn (7) for the triangle Ω^e is:

$$\int_{\Omega^e} \sum_{i=1}^{2} hk_i \frac{\partial N_m^e}{\partial x_i} \frac{\partial N_l^e}{\partial x_i} d\omega \cdot H_m + \int_{\Omega^e} N_m^e N_l^e d\omega \cdot \dot{H}_m = -\int_{\Gamma^e} q_b N_l^e ds + \int_{\Omega^e} q_e N_l^e d\omega \quad l, m = n, p, q \tag{10b}$$

Γ^e being the contour of Ω^e. Furthermore, in this case, for the elements internal to Ω, the first term on the right-hand side of eqn (10b) gives no contribution to the mass of water entering Ω^e. As a consequence, it can be neglected.

Both eqns (10a) and (10b) may be written in the following matrix form:

$$A_{lm}^e H_m + B_{lm}^e \dot{H}_m = Q_l \qquad l, m = n, p, q \tag{11}$$

where A_{lm}^e and B_{lm}^e are 3 × 3 elemental matrices, and H_m and $\dot{H}_m$ indicate, respectively, the 3 × 1 vectors of the nodal piezometric head and the corresponding time derivative. Matrix A_{lm}^e takes into account the conductivity of the system, and the capacity matrix B_{lm}^e takes into account the volume of water stored in the subcontrol volume as a consequence of an unitary variation of the piezometric head. The terms of matrix A_{lm}^e are functions of H_m, whereas the terms of matrix B_{lm}^e are constant and depend only on the geometry of the elemental triangle Ω^e. Matrix B_{lm}^e becomes a diagonal matrix when the lumping approximation is applied. The 3 × 1 vector Q_n takes into account source-sink terms. By using for the variables h, k_i, and H the approximations expressed by eqn (9a), the terms of the matrices A_{lm}^e and B_{lm}^e can be expressed in closed polynomial form as a function of the nodal values of these variables.

The assemblage of eqn (11) for all the triangular elements Ω^e results in a set of quasi-linear algebraic differential equations formally similar to eqn (11). The integration in time of this set of equations, by using a classical FD method, allows one to compute the distribution in space and in time of the piezometric heads and, therefore, of the velocity of water.

4 NUMERICAL EXPERIMENTS

Numerical experiments were performed for comparing the performances of the different CVFE and Galerkin FE formulations of the DHM model. To this end, twelve formulations were considered, six of them formulated on the basis of the CVFE method (CV_1, CV_{1L}, CV_2, CV_{2L}, CV_3, and CV_{3L}) and six formulated on the basis of the Galerkin FE method (FE_1, FE_{1L}, FE_2, FE_{2L}, FE_3, and FE_{3L}). The formulations differ in the approximation used for the variables appearing in the integral of the flux term in eqns (10a) and (10b), where eqn (9a) or (9b) was used, and for having used, or not used, the lumping approximation in the accumulation term in the same eqns (10a) and (10b). Hereafter we will indicate by:

CV_1 and FE_1 the cases in which $hk_i \simeq \hat{hk}_i$,

CV_2 and FE_2 the cases in which $hk_i \simeq \bar{hk}_i$,

CV_3 and FE_3 the cases in which $hk_i \simeq \hat{hk}_i(\bar{h}) \equiv \tilde{hk}_i$

and by CV_{1L}, CV_{2L}, CV_{3L}, FE_{1L}, FE_{2L}, and FE_{3L} the six lumped formulations that differ from the previous six formulations for the application of the lumping approximation in the computation of the capacity matrix. All the numerical experiments were carried out for the hypothetical watershed basin shown in Fig.3, which presents two bed slopes, S_{01} and S_{02}, respectively, along the x_1 and x_2 directions.

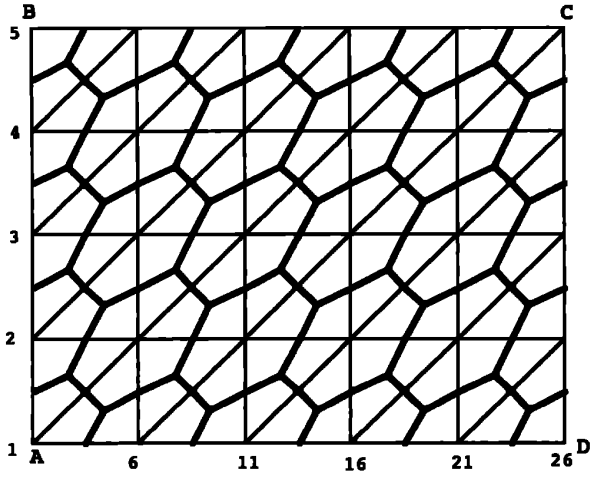

Fig. 3. FE grid (thin lines) and CV grid (thick lines) used for the test cases.

The boundary conditions for all cases were:

$q_{b_1}(t) = q_{b_2}(t) = 0$ along the sides BC and CD.

For all the test cases, the flow within the whole watershed basin was subcritical, so, along the sides AB and AD, the flow boundary condition in eqn (10) was calculated by supposing that the depth h varies linearly along the contour nodes and the outflow is expressed by:

$$q_b = (h^3 g)^{1/2} \tag{12}$$

where h is the critical depth and q_b is the specific outflow. The initial conditions for the whole basin were:

$$h(x_1, x_2, 0) = h_0(x_1, x_2) \tag{13}$$

It should be noted that the initial condition $h_0(x_1, x_2) = 0$ is not applicable, and we therefore used $h_0(x_1, x_2) = 1 \times 10^{-6}$ m for all the cases. In the following, i_e denotes the uniform rainfall intensity within the catchment basin, t_r and t_f denote the rainfall duration and the simulation time, and n_1 and n_2 denote the Manning roughness coefficients in the x_1 and x_2 directions. In order to obtain comparable results, for all the examples, the set of discrete-time equations was solved by using an FD-centered-in-time FD scheme, a minimum time step = 2 s, a maximum time step = 20 s, and a convergence-tolerance parameter = 10^{-3}. All the runs were done by using a Macintosh IIfx computer.

Test case 1

In this overland-flow test, we compare the numerical results of 24 runs with the analytical kinematic solution given by Stephenson and Medow.[17] The first twelve runs were performed for a low-slope basin ($S_{o1} = 0$, $S_{o2} = 0.0005$), whereas, for the other twelve runs, the slope of the basin was increased twenty times ($S_{o1} = 0$, $S_{o2} = 0.01$).

In S.I. units, the analytical solution of the kinematic wave model, developed for runoff from an impermeable rectangular plane for $t_c < t_f$, is:

$$t_c = (L/\alpha i_e^{m-1})^{1/m} \tag{14a}$$

$$q = \alpha (i_e t)^m \quad \text{for } 0 \le t \le t_c \tag{14b}$$

$$q = \alpha (i_e t_c)^m \quad \text{for } t_c < t \le t_r \tag{14c}$$

$$q = i_e L - i_e m \alpha^{1/m} q^{(m-1)/m} (t - t_r) \quad \text{for } t_r < t \le t_f \tag{14d}$$

$$\alpha = S_o^{1/2}/n; \qquad m = 5/3 \tag{14e}$$

where t_c is the time of concentration (i.e. the time that the rain-depth profile takes to reach the equilibrium condition), L is the length of the rectangle measured in the direction of the maximum slope, q is the discharge rate per unit width, S_o is the bed slope, and n is the Manning roughness coefficient.

For the first twelve runs (denoted by the numbers 1–12 in Table 1), the following data were used: $S_{o1} = 0$, $S_{o2} = S_o = 0{\cdot}0005$, $n_1 = n_2 = n = 0.020\ \text{m}^{-1/3}\text{s}$, $i_e = 0.33$ mm/min in the time interval 0–t_r, and $i_e = 0$ for $t > t_r$. For the subsequent twelve runs (denoted by the numbers 13–24 in Table 2), only the slope of the basin was increased twenty times ($S_{o1} = 0$, $S_{o2} = S_o = 0.01$).

Table 1. Global boundary-outflow errors, $e(t_r)$ and $e(t_f)$, with reference to the analytical solution, and CPU times for the Test Case 1, examples 1–12

Example	Algorithm	$e(t_r)$ %	$e(t_f)$ %	CPU [s]
1	$CV_{\cdot}$	2.09	1.33	476
2	$CV_{\cdot L}$	2.16	0.78	492
3	CV_2	1.63	0.71	454
4	CV_{2L}	1.77	0.19	471
5	CV_3	0.87	0.35	440
6	CV_{3L}	1.09	0.87	438
7	FE_1	0.09	1.01	434
8	$FE_{\cdot L}$	0.39	1.57	418
9	FE_2	1.03	0.19	392
10	FE_{2L}	1.29	0.46	370
11	FE_3	0.24	0.89	354
12	FE_{3L}	1.29	0.46	347

Table 2. Global boundary-outflow errors, $e(t_r)$ and $e(t_f)$, with reference to the analytical solution, and CPU times for Test Case 1, examples 13–24

Example	Algorithm	$e(t_r)$ %	$e(t_f)$ %	CPU [s]
13	$CV_{\cdot}$	2.32	0.96	514
14	CV_{1L}	2.24	0.98	523
15	CV_2	3.24	0.04	474
16	CV_{2L}	2.76	0.40	488
17	CV_3	4.67	1.84	446
18	CV_{3L}	3.07	0.24	479
19	FE_1	7.98	5.34	458
20	$FE_{\cdot L}$	3.51	0.82	427
21	FE_2	4.74	1.52	399
22	FE_{2L}	3.01	0.08	377
23	FE_3	7.74	5.05	372
24	FE_{3L}	3.45	0.75	357

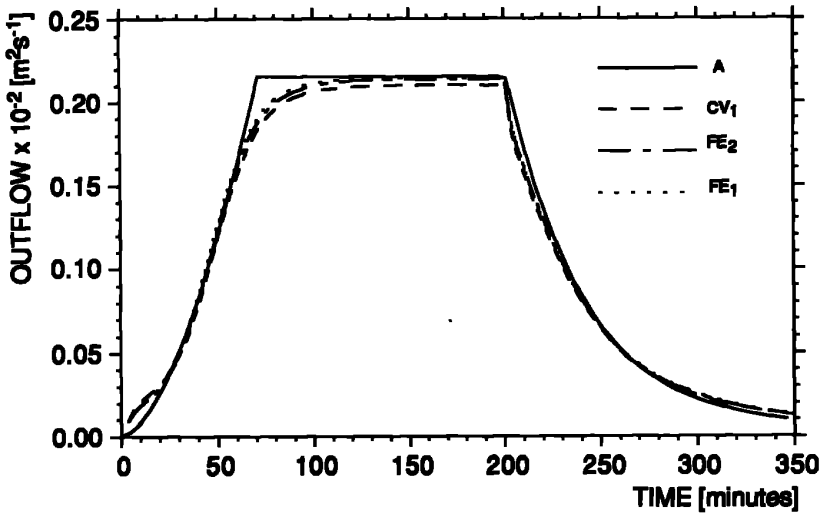

Fig. 4. Hydrographs in section 11 for the analytical solution and for CV_1, FE_2, and FE_1 methods (examples 1, 9, and 7).

In Figs 4, 5, 6, and 7 we show the hydrographs for the section (100 metres in length), associated with the node 11 along the side AD in Fig. 3. The hydrographs in Fig. 4 refer, respectively, to the analytical solution obtained by eqns (14), and to the CV_1, FE_2, and FE_1 formulations, whereas those in Fig. 5 refer to the analytical solution and to the CV_{1L}, FE_{2L}, and FE_{1L} lumped formulations. Global boundary-outflow errors with reference to the analytical solution at times t_r and t_f and CPU execution times are given in Table 1.

Figs 4 and 5 show that both the lumped and not-lumped approximations match very well with the analytical solution. The same is true for all the other six approximations not presented here for reasons of space. With regard to the global outflow-boundary errors, given in Table 1, it is possible to note that all CV and FE methods present small outflow errors.

The hydrographs in Fig. 6 refer, respectively, to the analytical solution obtained by eqns (14), and to the CV_1, FE_2, and FE_1 formulations, whereas the hydrographs in Fig.7 refer to the analytical solution and to the CV_{1L}, FE_{2L} and FE_{1L} lumped formulations. For these tests (examples 13–24), the global boundary-outflow errors with reference to the analytical solution at times t_r and t_f and CPU execution times are given in Table 2.

As can be seen from Figs 6 and 7, both lumped and not lumped approximations show a match with the analytical solution that is worse than that obtained in the previous cases with a lower slope. The same is true for all the other six approximations not presented in the

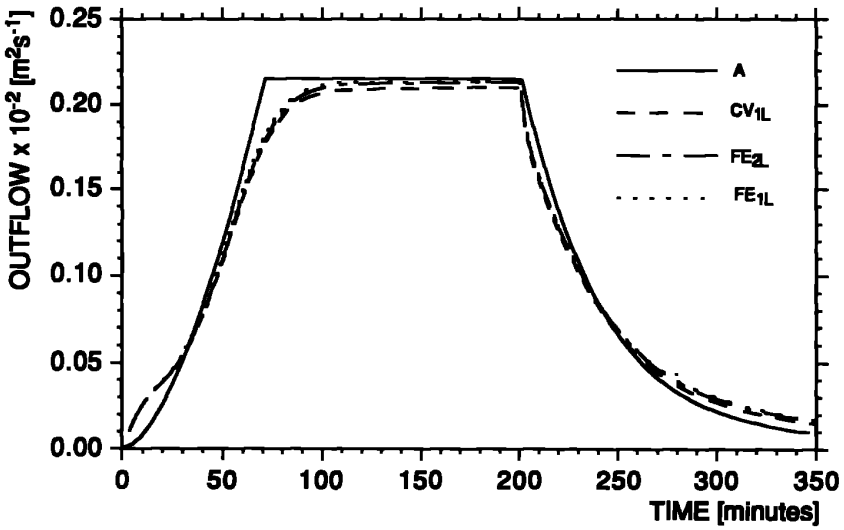

Fig. 5. Hydrographs in section 11 for the analytical solution and for CV_{1L}, FE_{2L}, and FE_{1L} methods (examples 2, 10, and 8).

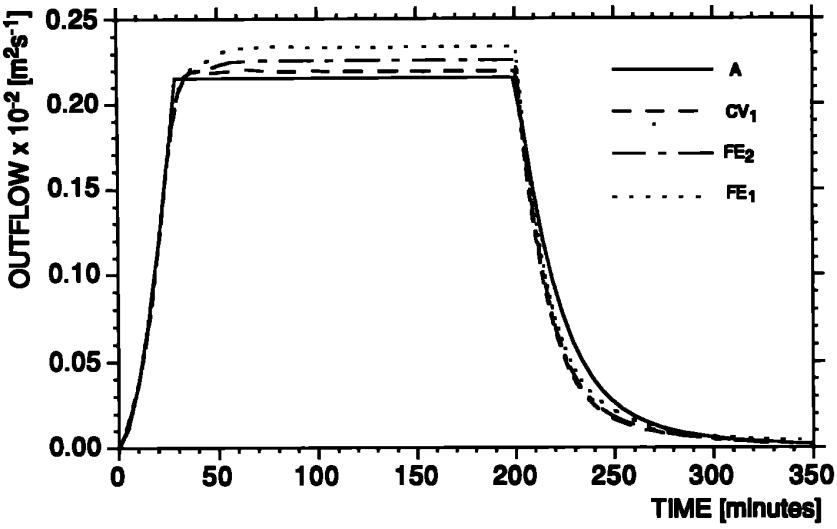

Fig. 6. Hydrographs in section 11 for the analytical solution and for CV_1, FE_2 and FE_1 methods (examples 13, 21, and 19).

graphs here. With regard to the global boundary-outflow errors, given in Table 2, it is possible to note that the CV methods exhibit smaller errors than the FE methods and also that the lumping approximation is more efficient in the FE than in the CV methods. From Fig. 7, we also note that the lumping approximation results in hydrographs showing an overshoot at concentration time. We conclude that the lumping approximation must be used only in the cases where the propagation velocity does not result in an oscillating solution (see Fig. 7).

Test case 2

This test case consists of twelve runs (denoted by the numbers 25–36 in Table 3), in which the following data

Table 3. Percentage differences, $e(t_r)$ and $e(t_f)$, in global-boundary outflow with reference to the CV_1 method, and related CPU times (Test Case 2)

Example	Algorithm	$e(t_r)$ %	$e(t_f)$ %	CPU (s)
25	CV_1	0.00	0.00	536
26	CV_{1L}	0.72	2.02	513
27	CV_2	0.31	2.23	537
28	CV_{2L}	0.54	2.38	498
29	CV_3	1.32	5.04	482
30	CV_{3L}	0.29	3.99	504
31	$FE_{:}$	3.40	7.25	489
32	$FE_{:L}$	0.68	4.61	459
33	FE_2	0.34	2.94	513
34	FE_{2L}	0.31	2.77	451
35	FE_3	2.97	7.17	445
36	FE_{3L}	0.61	4.55	430

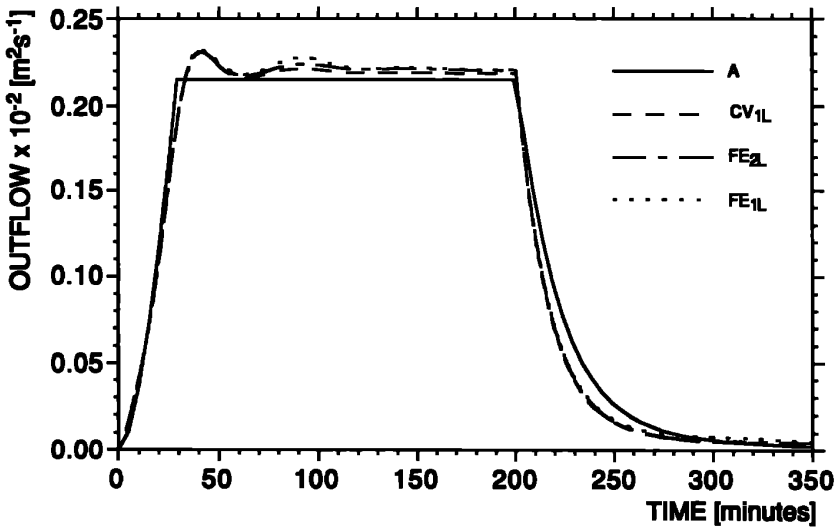

Fig. 7. Hydrographs in section 11 for the analytical solution and for CV_{1L}, FE_{2L}, and $FE_{:L}$ methods (examples 14, 22, and 20).

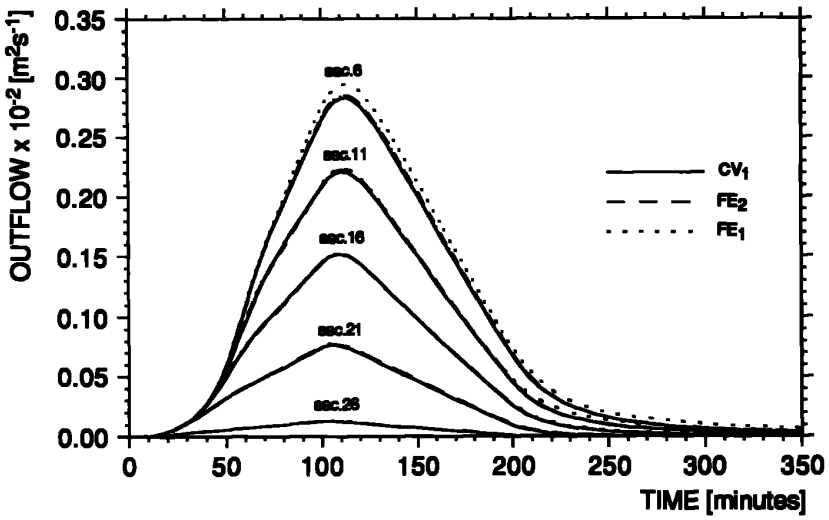

Fig. 8. Hydrographs in the section 6, 11, 16, 21, and 26 for the CV_1, FE_2, and FE_1 methods (examples 25, 33, and 31).

were used: $S_{o1} = S_{o2} = 0{\cdot}005$, $n_1 = n_2 = 0{\cdot}020\ \mathrm{m}^{-1/3}\mathrm{s}$. The rain intensity $i_e(t)$ in the interval 0–t_r is given by a triangular hyetograph defined by $i_e(0) = i_e(t_r) = 0$ and $i_e(t_r/2) = 0.48$ mm/min; $i_e = 0$ in the time interval t_r–t_f, where $t_r = 200$ min and $t_f = 350$ min.

Global-boundary-outflow percentage discards from the CV_1 method at times t_r and t_f and CPU execution times for these runs are given in Table 3. In Fig. 8, the hydrographs for the sections associated with the nodes along the side AD (nodes 6, 11, 16, 21, and 26) are given.

The graphs refer to the CV_1, FE_2, and FE_1 formulations. As can be seen from this figure, the match between the CV_1 and FE_2 formulations is excellent. On the contrary, the match of the FE_1 with the CV_1 and FE_2 formulations is only fair. By inspection of the results, given in Table 3, it is also possible to see that the CV and FE methods give errors that are remarkably different (see CV_1 and FE_1 methods).

5 CONCLUSIONS

Different CVFE and FE formulations for the numerical integration of a two dimensional DHM have been presented. A number of test cases using these formulations, along with some comparisons with a kinematic analytical solution, have been presented. From the results of the numerical experiments, carried out by using the different formulations, the following main conclusions can be drawn.

(i) As far as grid construction is concerned, the CVFE method offers the same flexibility as the FE method but allows a better physical interpretation of the discretized mass-balance equations.

(ii) The numerical solutions give a good match with the analytical kinematic solution.

(iii) The formulations based on the CVFE method (CV_1, CV_2, CV_3, and CV_{1L}, CV_{2L}, CV_{3L}) present global-boundary-outflow errors that are, in general, smaller than those of the corresponding FE formulations (FE_1, FE_2, FE_3, and FE_{1L}, FE_{2L}, FE_{3L}).

(iv) The use of the lumping approximation in the computation of the capacity matrix improves, in general, the global-boundary-outflow error in both the CVFE and FE methods. In particular, the improvement is more remarkable in the FE methods than in the CV methods.

(v) On the basis of the global-boundary-outflow errors, the CV and FE methods that use the approximation $hk_i \simeq \hat{hk}_i$ give the best results.

(vi) As could be expected, for the same mesh and time-step size, the increase in the propagation velocity, due to a rise in slopes or in rainfall intensity, causes, in general, an increase in the global boundary outflow error. For the lumped formulations, too high velocities can also originate oscillating solutions.

REFERENCES

1. Abbott, M. B., *Computational Hydraulics. Elements of the Theory of Free Surface Flows*, Pitman, London, 1979.
2. Akan, A.O. & Yen, B.C., Diffusion-wave flood routing in channel networks. *J. Hydraul. Div. ASCE*, **107(HY6)** (1981) 719–32.
3. Chow, V.T. & Ben-Zvi, A., Hydrodynamic modelling of two-dimensional watershed-flow *J. Hydraul. Div. ASCE*, **99(HY1)** (1973), 2023–40.
4. Connor, J.J. & Brebbia, C.A., *Finite Element Techniques for Fluid Flow*. Newnes-Butterworths, London, 1976.
5. Cunge J. A., Holly, F.M., jun. & Verwey, A., *Practical Aspects of Computational River Hydraulics*, Pitman, London, 1980.

6. De Vries, J.D., Hromadka, T.V. & Nestlinger, A.J., Applications of a two-dimensional diffusion hydrodynamic model *HYDROSOFT 86—Hydraulic Engineering Software*. In Proceedings of 2nd International Conference, Southampton, UK, 1986, pp. 393–412.
7. Fennemma, R.J. & Chaudry, M.H., Implicit methods for two-dimensional unsteady free-surface flows, *J. Hydraul. Res.*, **27** (1989) 321–32.
8. Forsyth, P.A., A control-volume, finite-element method for local mesh refinement in thermal reservoir simulation, *Soc. Pet. Eng. Res. Eng.*, **5** (1990) 561–6.
9. Fung, L.S., Hiebert, A.D. & Nghiem, L.X., Reservoir simulation with a control-volume finite-element method. *Soc. Pet. Eng. Res. Eng.*, **7** (1991) 349–57.
10. Gottardi, G. & Dall'Olio, D., A control-volume finite element model for simulating oil–water reservoirs. *J. Pet. Sci. Engng*, **8** (1992) 29–41.
11. Henderson, F.M., *Open Channel Flow*. Macmillan London, 1966.
12. Hromadka, T.V., Berenbrock, C.E., Freckleton, J.R. & Guymon, G.L., A two-dimensional dam-break flood plain model. *Adv. Water Resour.*, **8** (1985) 7–14.
13. Hromadka, T.V., McCuen, R.H. & Yen, C.C., Comparison of overland flow hydrograph models, *J. Hydraul. Div. ASCE*, **113(HY11)** (1987) 1422–40.
14. Katopodes, N.D. & Strelkoff, T., Computing two-dimensional dam-break flood waves. *J. Hydraul. Div. ASCE*, **104(HY9)** (1978) 1269–88.
15. Katopodes, N.D. & Strelkoff, T., Two-dimensional shallow water-wave models. *J. Mech. Div. ASCE*, **105(EM2)** (1979) 317–34.
16. Narasimhan, T.N. & Witherspoon, P.A., An integrated finite difference method for analyzing fluid flow in porous media. *Water Resour. Res.*. **12** (1976) 57–64.
17. Stephenson, D. & Meadows, M.E., *Kinematic Hydrology and Modelling*. Elsevier Science Publishers, New York, NY, USA, 1986.
18. Xanthopoulos, Th. & Koutitas, Ch., Numerical simulation of two-dimensional flood wave propagation due to dam failure, *J. Hydr. Res.*, **14** (1976) 321–31.